J. Fluid Mech. (2012), *vol.* 706, *pp.* 323–350.
doi:10.1017/jfm.2012.255

Determining the stability of steady two-dimensional flows through imperfect velocity-impulse diagrams

P. Luzzatto-Fegiz† and C. H. K. Williamson

Sibley School of Mechanical and Aerospace Engineering, Cornell University, Ithaca, NY 14853, USA

(Received 21 October 2010; revised 16 February 2012; accepted 25 May 2012;
first published online 13 July 2012)

In 1875, Lord Kelvin stated an energy-based argument for equilibrium and stability in conservative flows. The possibility of building an implementation of Kelvin's argument, based on the construction of a simple bifurcation diagram, has been the subject of debate in the past. In this paper, we build on work from dynamical systems theory, and show that an essential requirement for constructing a meaningful bifurcation diagram is that families of solutions must be accessed through isovortical (i.e. vorticity-preserving), incompressible rearrangements. We show that, when this is the case, turning points in fluid impulse are linked to changes in the number of the positive-energy modes associated with the equilibria (and therefore in the number of modes likely to be linearly unstable). In addition, the shape of a velocity-impulse diagram, for a family of solutions, determines whether a positive-energy mode is lost or gained at the turning point. Further to this, we detect bifurcations to new solution families by calculating steady flows that have been made 'imperfect' through the introduction of asymmetries in the vorticity field. The resulting stability approach, which employs 'imperfect velocity-impulse' (IVI) diagrams, can be used to determine the number of positive-energy (likely unstable) modes for each equilibrium flow belonging to a family of steady states. As an illustration of our approach, we construct IVI diagrams for several two-dimensional flows, including elliptical vortices, opposite-signed vortex pairs (of both rotating and translating type), single and double vortex rows, as well as gravity waves. By also considering an example involving the Chaplygin–Lamb dipole, we illustrate how the stability of a specific flow may be determined, by embedding it within a properly constructed solution family. The stability data from our IVI diagrams agree precisely with results in the literature. To the best of our knowledge, for a few of the flows considered here, our work yields the first available stability boundaries. Further to this, for several of the flows that we examine, the IVI diagram methodology leads us to the discovery of new families of steady flows, which exhibit lower symmetry.

Key words: bifurcation, variational methods, vortex instability

† Physical Oceanography Department, Woods Hole Oceanographic Institution, Woods Hole, MA 02543, USA. Email address for correspondence: pluzzattofegiz@whoi.edu

1. Introduction

Over a century ago, Sir William Thomson (now more widely known as Lord Kelvin) proposed an energy argument for determining equilibrium and stability in an inviscid, homogeneous flow (a printed version of his 1875 contribution to a meeting of the Royal Society of Edinburgh appeared as Thomson 1876). Thomson stated his argument without proof; the first analytical confirmation of his ideas is traditionally attributed to Arnol'd (1966) or Benjamin (1976). Kelvin considered flows that are steady when observed in a reference frame that is translating or rotating with constant velocity, and proposed that any such flow corresponds to a stationary value of the energy, under perturbations that preserve vorticity and impulse (see § A.1 for a mathematical outline). Kelvin went on to note that, for flows that conserve energy, the link between stationary points of the energy and steady flows has important consequences for stability. If the steady flow corresponds to a maximum or minimum of the energy, a displacement of the system away from the equilibrium point would require a change of energy, which is impossible. Hence the equilibrium flow must be stable. By the same reasoning, a necessary condition for instability is that the flow must correspond to a saddle of the energy. This idea is at the core of the well-known stability theorems of Arnol'd (1965, 1966), and forms the basis of several stability methodologies (e.g. Holm *et al.* 1985).

However, the application of these energy-based ideas to determine stability is often limited by practical considerations, since one has to evaluate the second-order change in energy (that is, the second variation) for all admissible perturbations. This may be possible for certain flows that admit explicit analytical solution. On the other hand, computing the second variation of the energy for a numerically obtained flow is prohibitively difficult, as one has to consider a second-order expansion involving an infinite number of possible perturbations (as discussed by Dritschel 1985). This issue places a severe limitation on the practical implementation of Kelvin's argument.

Seeking to circumvent this difficulty, Saffman & Szeto (1980, 1981) proposed a different implementation of Kelvin's argument. We summarize here the approach followed in their 1980 paper. Saffman and Szeto computed numerically a family of steady, co-rotating vortex pairs, having equal area and uniform vorticity. Having obtained the steady states, they calculated their energy E and angular impulse J. In an attempt to heuristically deduce which solutions represented maxima of the energy, for a given impulse, they examined possible values of E, for a given J; for their family of solutions, they found that the solutions displayed a simultaneous turning point in E and J (as schematically shown in figure 1). Saffman & Szeto (1980) then proposed that the 'highest' curve in the plot would be a maximum in E (for a given impulse J), while the lower branch would likely be a saddle of E. Hence the top branch would be stable, the lower branch would likely be unstable, and the connection between the two branches could correspond to a change of stability. For this flow, Kamm (1987) and Dritschel (1995) later found that the stability boundary obtained from a (J, E) plot agreed with detailed linear stability calculations.

However, the approach proposed by Saffman & Szeto (1980) is affected by a number of issues. Two problems were first pointed out by Dritschel (1985), in a seminal paper on the stability of vortex arrays. Firstly, Dritschel (1985) observed the absence of a rigorous link between the properties of the energy surface and the shape of an energy-impulse plot. Secondly, Dritschel (1985) remarked that, even if such a link could be firmly established, additional changes of stability could also occur away from extrema in E and J, by means of bifurcations to (hitherto undiscovered) families of solutions (illustrated schematically in figure 1*b*). This

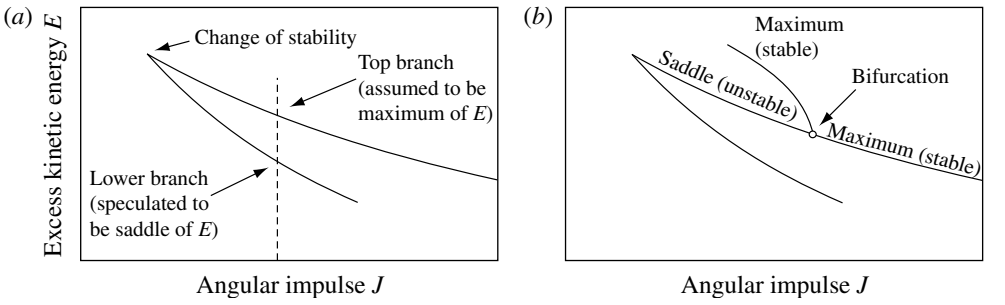

FIGURE 1. Sketch of impulse and excess energy for a co-rotating vortex pair, illustrating the approach of Saffman & Szeto (1980).

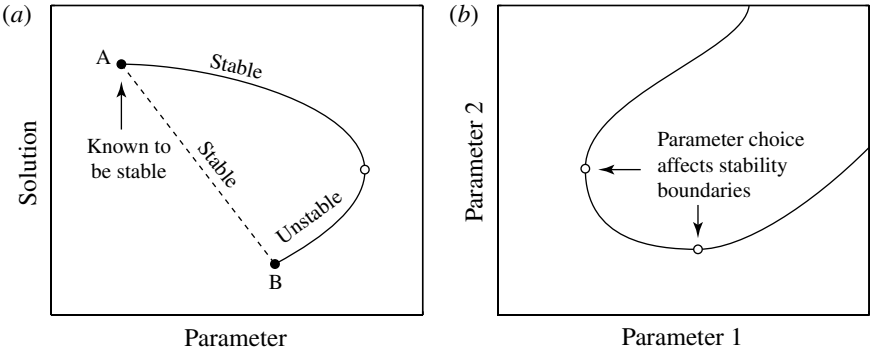

FIGURE 2. Sketches illustrating two issues associated with turning-point approaches for vortex flows, which may lead to inconsistencies in the stability boundaries: (*a*) dependence on how the family of solutions is constructed, (*b*) dependence on choice of control parameter.

point was corroborated by the numerical stability findings on opposite-signed vortex pairs reported in Dritschel (1995). These results led Dritschel (1995) to conclude, regarding Saffman's interpretation of Kelvin's ideas, that 'the argument, based on Kelvin's variational principle … that the margin of stability can be decided from the $E(J)$ curve alone … does not always work'. As a consequence of these two concerns, the stability method proposed by Saffman & Szeto (1980) has since been considered unreliable (D. Crowdy, 2008, private communication); indeed, to the best of our knowledge, energy-impulse plots have not been employed in any other vortex dynamics studies to date.

In addition to the two issues summarized above, we note here two additional problems, which do not seem to have been previously recognized. These concern: (i) the rules used to build solution families; and (ii) the choice of a physically relevant parameter to characterize solutions. To expand on the first point, one can note that since fluid problems are typically infinite-dimensional, any two distinct vortex flows may be connected through an infinite number of possible paths, involving series of intermediate solutions. The presence (or absence) of turning points can be intuitively seen to depend on the choice of path, as sketched in figure 2(*a*). Point (ii) above can also be appreciated through a simple schematic illustration, in figure 2(*b*), showing that different choices of control parameter can lead to inconsistent stability predictions. We feel that the need for clarification on these two points is well exemplified by

considering a statement appearing in the monograph of Saffman (1992, p. 191). This considers the stability of the family of Stuart vortices, which can be written in closed form as a function of a parameter C: 'the absence of a transition (to instability) is associated with the non-existence of a fold or limit point in the properties of the family of Stuart vortices, as C decreases from ∞ to 1'. As we deduce in appendix A, Stuart vortices do not actually form a family that is amenable to a turning point analysis. In addition, the chosen parameter C is not necessarily a control parameter that is meaningful for stability calculations.

We were motivated to re-examine this problem by the fact that a simple stability approach, based on the construction of a suitable bifurcation diagram, could be valuable in a wide range of applications. For example, we note here that several debates (each spanning at least a decade) have existed over the stability of comparatively simple flows. Examples include co-rotating vortex pairs (Saffman & Szeto 1980; Dritschel 1985; Kamm 1987; Saffman 1992; Dritschel 1995), streets of finite-area vortices (see Meiron, Saffman & Schatzman 1984, Jiménez 1987, and references therein), as well as ellipsoidal vortices in quasigeostrophic flows (Dritschel, Scott & Reinaud 2005, and references therein). Similar debates have also unfolded over the stability boundaries of steep gravity waves, where the first (erroneous) application of a turning-point argument appears to date back to Stokes (1879) (for more on this problem, see Saffman 1985, and references therein). It is conceivable that a simple stability approach, beside proving valuable in its own right, could also be used to quickly confirm correct results from linear analysis, and question possibly spurious ones. A bifurcation-diagram stability methodology could therefore complement more involved approaches, such as linear analysis or time-dependent simulations, which would yield additional information about growth rates and long-term evolution of the flow.

This paper is structured as follows. Section 2 briefly outlines, in a heuristic manner, the key physical ideas underlying the construction of a turning-point approach for vortex flows; the mathematical underpinnings are relegated to appendix A. In § 3, we propose to seek bifurcations of steady vortical families by introducing ideas from the study of imperfect dynamical systems. Several examples involving two-dimensional vortical flows are examined in § 4. As an example involving a different type of flow, in § 5 we look at steep gravity waves. A brief discussion of the numerical results follows in § 6. Finally, in § 7, we discuss possible future applications of the stability method, as well its applicability in conjunction with other, more complex approaches.

2. Linking velocity-impulse diagrams and stability properties

We briefly discuss here the key notions underlying the construction of a turning point approach for vortex flows, as is necessary to introduce the examples in §§ 4 and 5. The mathematical details are contained in appendix A.

In the first instance, we consider the choice of control parameter. Equilibrium vortex calculations are usually parametrized by the velocity of the configuration (e.g. Deem & Zabusky 1978) or by a geometric measure of the proximity of the vortices (e.g. Makarov & Kizner 2011). However, we argue here that a selected control parameter, chosen to be relevant to stability studies, must be constant through the unsteady evolution of the flow; as such, we propose using the fluid impulse, which is a conserved quantity in an inviscid fluid (e.g. Saffman 1992).

Secondly, we consider the problem of organizing vortical solutions into families. By introducing methods from dynamical systems theory, we find that families of

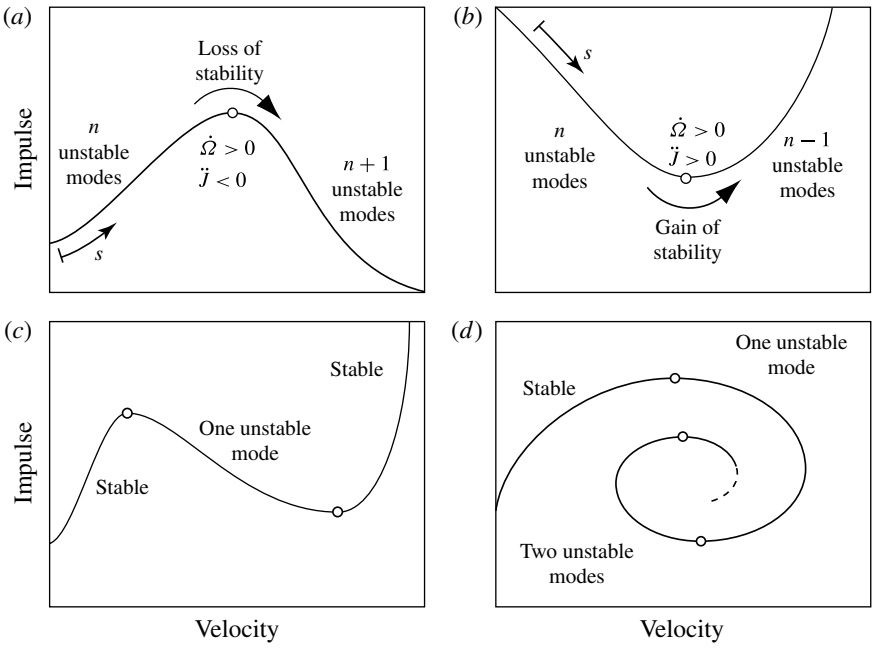

FIGURE 3. Schematic velocity-impulse diagrams. A maximum or minimum of the impulse is associated with the addition or subtraction of a positive-signature mode, respectively, as the curve is traversed from left to right (see appendix A).

solutions must be built through a rearrangement of the same type as the rearrangement used for Kelvin's argument. As discussed in appendix A, this implies that solution families must be built from incompressible, isovortical (i.e. vorticity-preserving) rearrangements.

To the best of our knowledge, these two points above do not appear to have been previously recognized in the vortex dynamics literature. It is easy to verify that the Stuart family, discussed by Saffman (1992), cannot be traversed through isovortical rearrangements. For example, one may note that the limit $C \to \infty$ yields a row of point vortices, which cannot be rearranged into any of the smooth vorticity distributions obtained for finite C.

As mentioned in § 1, if one can show that, for all incompressible and isovortical perturbations, the second variation of the energy is always negative (implying the energy is a maximum), then the equilibrium is stable. (An energy minimum is similarly stable, but is not realizable in an unbounded flow, and is therefore not discussed here; e.g. Thomson 1880*a*.) To detect a switch from maximum to a saddle, it is therefore of interest to search for the onset of any modes that have a positive second variation (such modes are said to have positive energy signature, or simply 'positive signature'; e.g. Arnol'd & Avez 1968). As we show in appendix A, properly constructed solution families have a zero-signature mode at a turning point in impulse, indicating a possible change in energy signature. Further to this, we show that the direction of the change of signature (from negative to positive, or vice versa) can be inferred from the shape of a velocity-impulse plot, as illustrated in figure 3. If the equilibria on one side of the fold already have one positive-energy mode, this result enables us to distinguish whether a positive-signature mode is added or subtracted

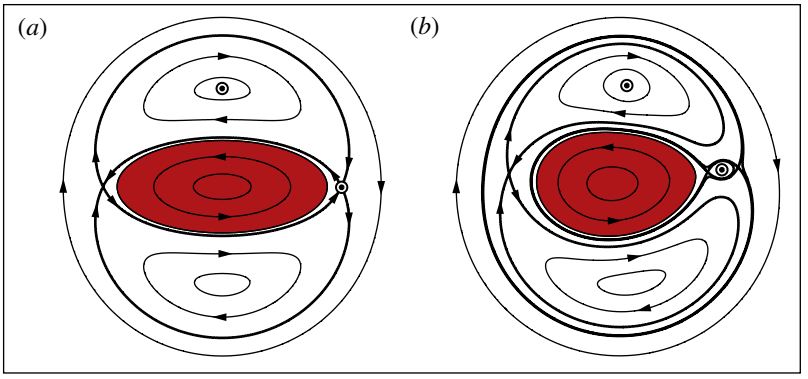

FIGURE 4. Illustration of the effect of introducing a symmetry-breaking imperfection, for a vortical flow. (*a*) The streamlines of the flow field in the reference frame that is co-rotating with the elliptical vortex shape. In order to break the symmetry in the flow, we introduce point vortices at certain stagnation points (marked by the bull's eyes), and seek the vortex shape and point vortex positions yielding a steady flow.

(thereby yielding flows that are likely to have more or fewer linearly unstable modes, respectively).

3. Introducing imperfections to reveal bifurcations in steady flows

Let us now consider the problem of detecting a bifurcation to a new family of steady solutions. The velocity-impulse diagram introduced in § 2 is, by itself, insufficient to find these situations, as they are not associated with turning points in a control parameter. This is, in essence, the second objection raised by Dritschel (1985), which applies to any stability approach based exclusively on the use of turning points.

However, a basic result from singularity theory is that bifurcations connecting different families of steady solutions are not robust under small changes in the governing equations, and will instead break into distinct branches, ultimately giving rise to turning points (e.g. Poston & Stewart 1978). The effects of this structural instability have been observed across a wide range of areas of work, ranging from structural mechanics (Thompson 1975) to the growth of viscous fingers at the interface between two fluids (Casademunt & Jasnow 1991), to capillary bridges (Lowry & Steen 1995). To the best of our knowledge, this use of imperfections has not been attempted before in the study of vortex dynamics.

For vortex flows, we propose an imperfection approach by focusing on breaking any reflectional or rotational symmetry exhibited by the steady flow. As an example, we consider here the steady elliptical vortices first found by Kirchhoff (1876); the associated streamlines, as seen in a frame of reference that is rotating with the vortex shape, are shown in figure 4(*a*). We choose to introduce a point vortex at each of the two stagnation points marked by a bull's eye in figure 4(*a*). We then proceed to re-compute the steady states. Note that this involves solving also for the locations of the stagnation points at which the point vortices are located. Figure 4(*b*) shows a case where a very strong imperfection has been employed, leading to a flow that, while steady, clearly lacks symmetry.

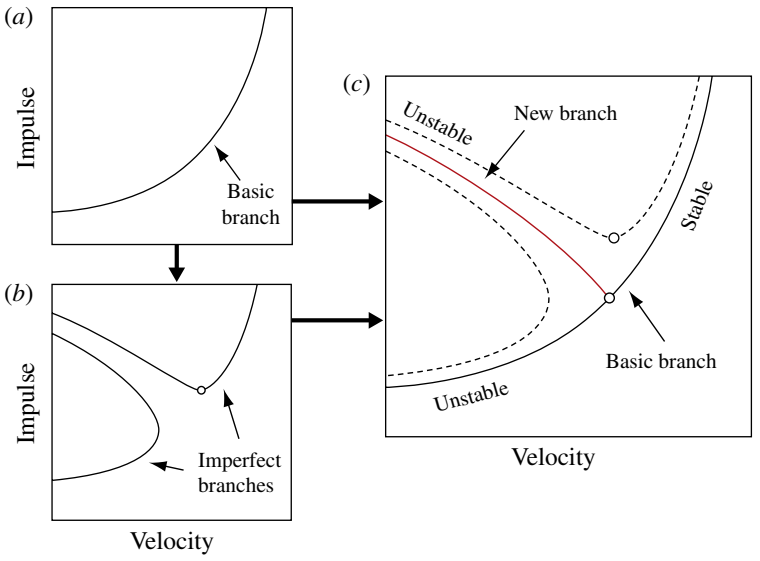

FIGURE 5. Sketch illustrating the process of constructing an imperfect velocity-impulse (IVI) diagram.

We must stress here that the *imperfection* involves the construction of a new, slightly asymmetric steady flow, which is closely related to a previously known, more symmetric equilibrium flow. In other words, this essentially involves the solution of a modified *equilibrium* problem. This is not to be confused with the introduction of a symmetry-breaking *perturbation*, which may lead to a *dynamical* behaviour that also exhibits similar symmetry breaking.

To consider the practical implementation of this idea, suppose we have computed a family of steady solutions numerically (as shown schematically in figure 5*a*), and wish to verify whether any bifurcations exist. We then introduce a symmetry-breaking imperfection, in the manner explained above; for all the examples that we consider, if a hidden branch exists, we find that the basic family is broken into two imperfect branches (figure 5*b*). By taking the strength of the point vortices back to zero, we recover the underlying bifurcated branch (shown as the red line in figure 5*c*). The turning points in the imperfect branches (which are now shown as dashed lines in figure 5*c*) can be used to diagnose stability for both the basic and the bifurcated branch.

It should be made clear that, for these fluid problems, there is no proof that such imperfections must capture all bifurcations. However, we have found that in all the examples we have studied so far (in this paper, as well as Luzzatto-Fegiz & Williamson 2010, 2011*b*) this use of imperfections correctly delivers all existing bifurcations, as verified by separate stability analyses.

4. Stability of two-dimensional vortical flows from IVI diagrams

In the two-dimensional vortical examples considered below, the velocity and impulse (defined in appendix A) of the configurations are normalized as (with unit density):

$$\Omega^* = \Omega\,\tilde{\omega}^{-1}, \quad U^* = U\,(\tilde{\Gamma}\tilde{\omega})^{-1/2}, \tag{4.1a}$$

$$J^* = J\,\tilde{\omega}\Gamma^{-2}, \quad I^* = I\,\tilde{\Gamma}^{-3/2}\tilde{\omega}^{1/2}, \tag{4.1b}$$

where Γ is the total circulation of the flow, $\tilde{\Gamma} = \int |\omega|\,\mathrm{d}A$ and $\tilde{\omega} = \max|\omega|$. For spatially periodic solutions of energy E, in a periodic cell of width L, we also employ

$$E^* = E\,\tilde{\Gamma}^{-2}, \quad L^* = L\,\tilde{\Gamma}^{-1/2}\tilde{\omega}^{1/2}. \tag{4.2}$$

Since our main focus here is on the stability methodology, we represent each flow through a collection of uniform-vorticity regions. The requirement that solutions must be built through incompressible, isovortical rearrangements is satisfied by fixing the area of uniform vorticity inside each patch. In spite of this simplification, accurate computation of steady uniform vortices remains non-trivial. Here we employ a recently developed numerical method, capable of calculating vortices of arbitrary shape, which features an adaptive discretization procedure to accurately resolve any fine-scale features that may arise; the details are reported in Luzzatto-Fegiz & Williamson (2011*a*).

4.1. *The Kirchhoff elliptical vortices*

The elliptical vortices discovered by Kirchhoff (1876) constitute a family of solutions that begins with a circular vortex and terminates with a vortex sheet (see Saffman 1992 for a modern treatment). These steady states can be characterized analytically; their impulse and velocity are related by $J^* = (2\Omega^* - 1)\,(8\pi\Omega^*)^{-1}$, where the angular velocity is related to the axis ratio $\lambda = b/a$ by $\Omega^* = \lambda\,(\lambda + 1)^{-2}$. Since $J^* = -\,(4\pi)^{-1}$ for the circular vortex, while $J^* \to -\infty$ as the vortex sheet solution is approached, we choose to plot $-\,(4\pi J^*)^{-1}$ instead of J^* (as shown in figure 6*a*). Since $J^*(\Omega^*)$ is monotonic, any positive-signature modes have to arise at bifurcations. (In general, the bifurcated branches will not admit an analytic representation.)

The initial configuration corresponding to a circular vortex can be argued to constitute an energy maximum (see Thomson 1880*b*). In order to search for bifurcations, we initialize our calculations by introducing an imperfection in a near-circular vortex, through the placement of two point vortices (of strength Γ_{PV}) at certain stagnation points of the co-rotating flow, as shown in figure 6(*d*). Their circulation is set to $\Gamma_{PV}/\Gamma = 10^{-4}$. We compute imperfect flows with progressively lower velocity and impulse. At $(\Omega^*, J^*) \doteq (0.18815, -0.13183)$, we encounter a turning point in impulse in the imperfect branch, after which J^* begins to increase, thus revealing the introduction of a positive-signature mode (this imperfect branch is shown by the right-hand dashed line in figure 6*c*).

We continue to seek bifurcations from the basic solution family by considering an elliptical vortex located shortly after the turning point described above (as we travel along the solution branch to smaller Ω^*), where we introduce the same imperfection again. This enables us to map the second imperfect branch, for both increasing and decreasing J^* (a portion of this branch is shown by the dashed line on the left-hand of figure 6*c*). By repeating this process, we detect the first three bifurcations, all of which turn out to correspond to the introduction of additional positive-signature (possibly unstable) modes, as marked in figure 6(*b*) by 1U, 2U, 3U, ...

By taking the strength of the point vortices to zero, we are able to recover the underlying bifurcated branches (shown by red lines in the figure), which are found to terminate with the limiting shapes shown in figure 6(*b*). The intersection between the bifurcated and original solution series yields the locations of the bifurcations.

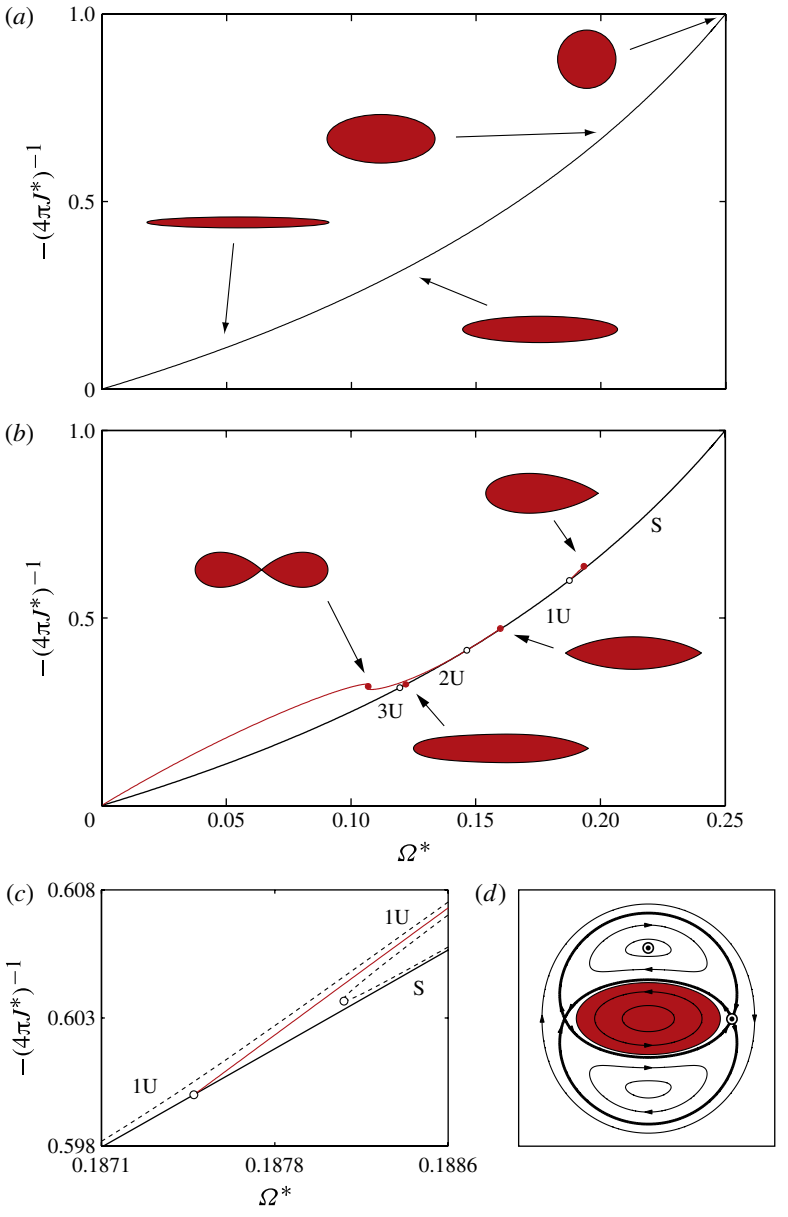

FIGURE 6. (*a*) The velocity-impulse plot for the Kirchhoff ellipses. We introduce imperfections by placing weak point vortices at certain stagnation points of the co-rotating flow (marked by bull's eyes $\odot$ in *d*). (*b*) The first three bifurcated branches found using this approach. (*c*) A close-up of the structure of the first bifurcation. Filled and empty circles denote limiting shapes and stability boundaries, respectively.

To conclude this section, we note that the locations of changes of stability presented here, obtained from an IVI diagram, match the results from the linear stability analysis of Love (1893) to at least seven significant figures. Love's analysis formed the basis of part of the work of Kamm (1987), who computed the beginning of the bifurcated

branches presented here; the second bifurcated branch (shown in red in figure 6*b*) was later explored in its entirety by Cerretelli & Williamson (2003). More detailed information about the IVI diagram for the elliptical vortices (including a different choice of imperfection) can be found in Luzzatto-Fegiz & Williamson (2010).

4.2. *The unequal-circulation pair*

We examine pairs of opposite-signed vortices having equal vorticity magnitude but unequal circulation. Flows of this type were first computed by Dritschel (1995). We consider here the family of solutions obtained for circulation ratio given by $\Gamma_2/\Gamma_1 = -0.3$.

It can be shown that a pair of well-separated vortices is a maximum of the energy, for a given impulse (Luzzatto-Fegiz & Williamson 2011*b*). As the vortices are brought closer together, one obtains the basic family of steady states shown in figure 7(*a*). We can immediately point out the addition of a positive-signature mode at a turning point in J^*. In order to seek out bifurcations, we break the reflection symmetry in the vorticity distribution shown in figure 7(*d*) by placing a point vortex at one of the saddle-type stagnation points of the co-rotating flow. The point vortex has strength, relative to the largest vortex, $\Gamma_{PV}/\Gamma_1 = 10^{-4}$. As we proceed to compute steady imperfect flows with progressively lower J^*, we discover a turning point in impulse at $(\Omega^*, J^*) \doteq (0.11426, -0.00405)$, which introduces an additional positive-signature mode (as shown by the close-up in figure 7*c*). Following a procedure similar to the one employed for the elliptical vortices, we computed the next imperfect branch, and sought additional bifurcations from the original family; however, we found none. For this flow, the bifurcated branch (shown in red in figure 7*b,c*) corresponds to a new family of vortices, whose shapes do not exhibit any symmetry. This family of solutions terminates with the limiting shape shown in figure 7(*b*).

The stability boundaries found from the IVI diagram turn out to match results from the linear analysis of Dritschel (1995). Furthermore, the IVI diagram delivers a new family of non-symmetric steady vortices (figure 7*b*), together with their stability properties.

4.3. *The equal-circulation pair*

This section focuses on the special case involving an opposite-signed vortex pair with equal vorticity and circulation magnitude. The basic family of solutions (shown in figure 8*a*) was first obtained by Pierrehumbert (1980). It should be noted that the limiting shape (first accurately computed by Saffman & Tanveer 1982) has a 'rugby ball' appearance, which is drastically different from the limiting shapes that one obtains for unequal-strength vortices (see figures 7*a* and 8*a*). This discrepancy persists as Γ_2/Γ_1 takes values close to -1. As noted by Dritschel (1995), reconciling these two solution series represents an outstanding question.

For this flow, we introduce an imperfection by letting the two vortices have slightly different areas (such that $\Gamma_2/\Gamma_1 = -0.995$), while also placing a point vortex at one of the saddle-type stagnation points, marked by a bull's eye in figure 8(*d*). The strength of the point vortex is fixed by the requirement that the configuration must still translate along a straight line, which in turn implies that the overall circulation must be zero (that is, $\Gamma_1 + \Gamma_2 + \Gamma_{PV} = 0$).

By starting with a well-separated pair, and following the imperfect branch to lower values of impulse, we discover a turning point for $(U^*, I^*) \doteq (0.10820, 0.27531)$, corresponding to the addition of a positive-signature mode (shown in detail in figure 8*c*). Continuing the search for new solution branches, we find a rich bifurcation

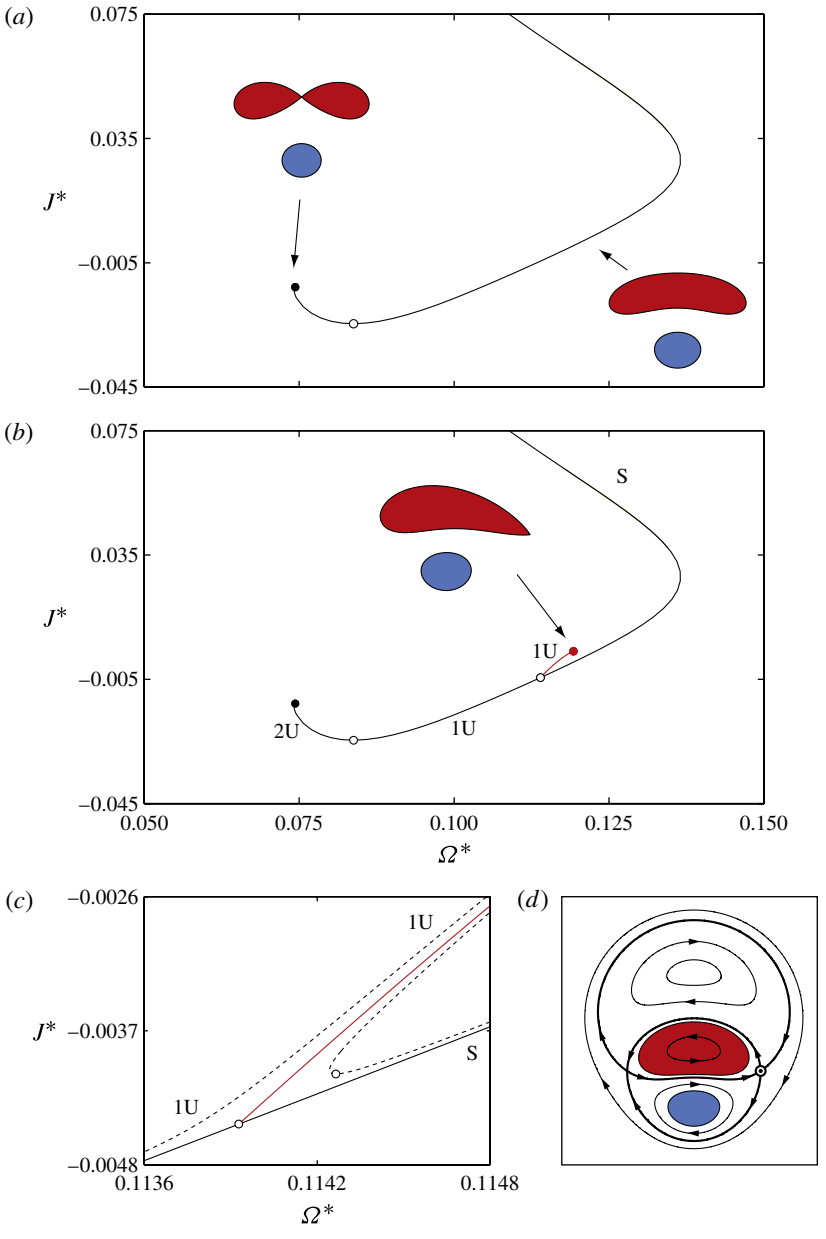

FIGURE 7. (*a*) The velocity-impulse diagram for the opposite-signed, uniform vortex pair with area ratio $A_1/A_2 = 0.3$. The imperfection is constructed by introducing a point vortex at the stagnation point marked by a bull's eye in (*d*). (*b*) A new family of vortices. (*c*) A close-up of the associated bifurcation.

structure. These further bifurcations are not reported here; we hope to give a detailed account of these results in a future contribution. The first bifurcation described above leads to a new family of steady vortices, shown by the red line in figure 8(*b*,*c*). We should stress that, in spite of their lower symmetry, these vortices translate along a straight line.

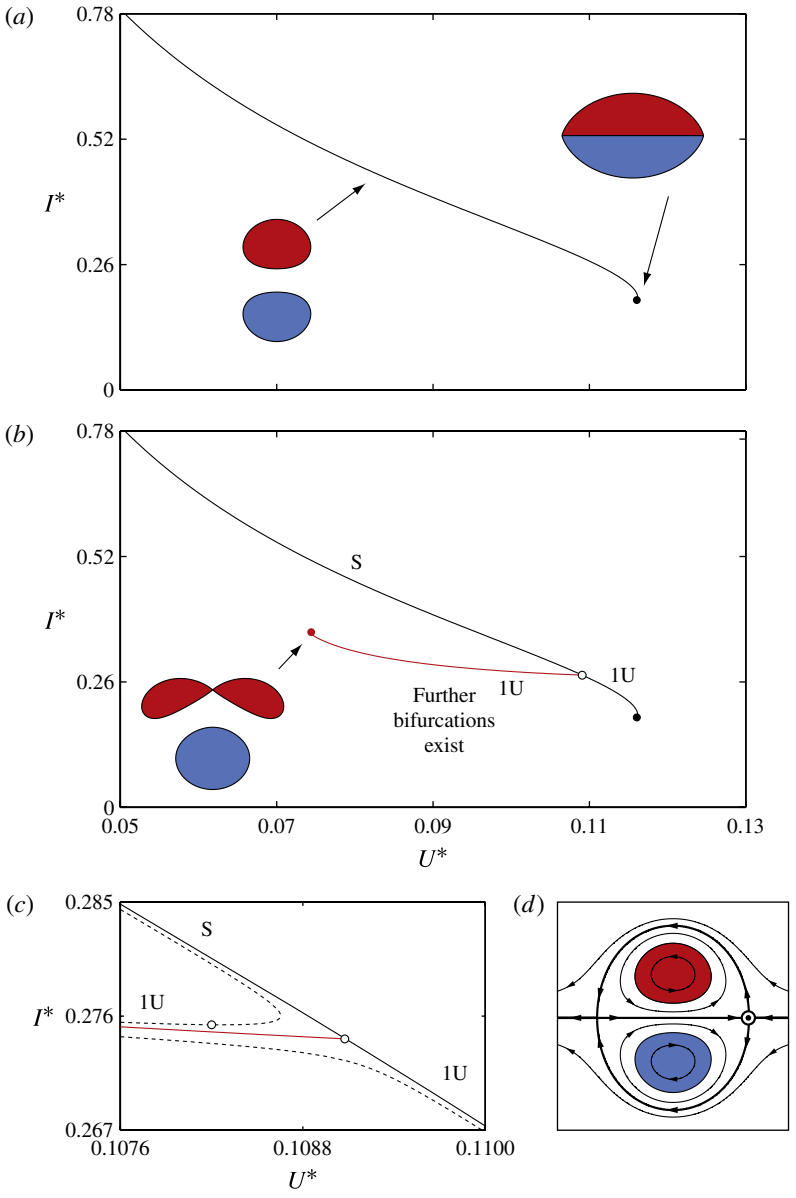

FIGURE 8. (*a*) The velocity-impulse plot for the equal-area, translating vortex pair. The symmetry of the flow is broken by decreasing the area of one of the two vortices, while also introducing a point vortex. (*b*) The IVI diagram shows the first bifurcation uncovered through this approach. (*c*) A close-up of the first bifurcation. Other bifurcations were detected through the IVI diagram approach; these are not shown here.

The location of the first loss of stability matches the stability boundary calculated by Dritschel (1995) through a linear analysis. The IVI diagram approach also leads us to the discovery of a new family of lower-symmetry vortices. Furthermore, we may recognize the limiting shape shown on the left of figure 8(*b*) as the equal-area version of the limiting state for the unequal-area vortices, seen in figure 7(*a*). We may

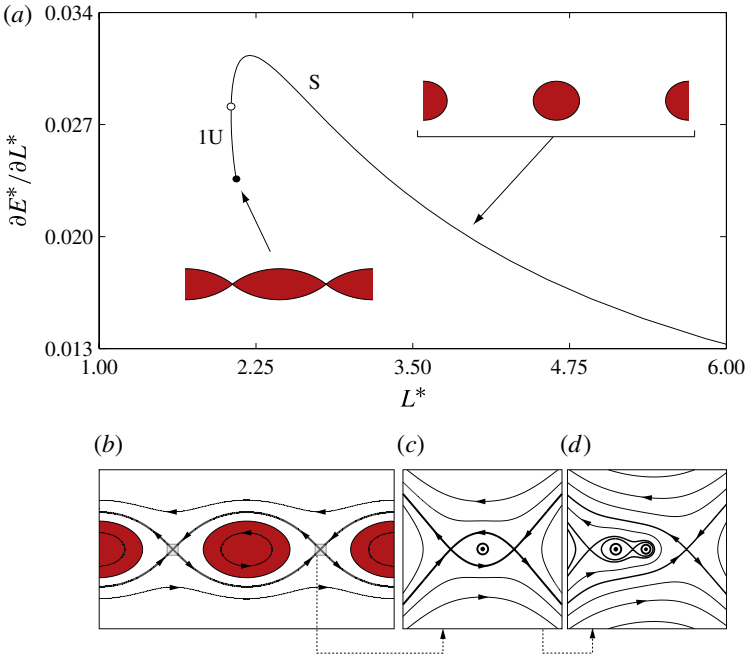

FIGURE 9. Stability of the linear vortex array, for superharmonic perturbations. The flow is made non-symmetric through a two-step process, as shown in (*b–d*). The neighbourhood of a stagnation point (highlighted by a grey box in *b*) is first altered by introducing a point vortex of strength Γ_{PV} (marked by the bull's eye in *c*), which changes the local flow topology. This creates two new stagnation points near the original one. Introducing a further point vortex at one of these locations (marked by the left-hand bull's eye in *d*) breaks the left/right symmetry. No bifurcations were found, consistently with classic stability results.

therefore interpret the unequal-area vortices of § 4.2 as the first imperfect branch of the equal-area family, for which the imperfection (in this case, the circulation difference between the vortices) has been brought to large values. Therefore the imperfection technique proposed here naturally reconciles the two families of solutions.

4.4. *The single vortex row*

We next examine a row of identical uniform vortices, whose centroids are separated by a non-dimensional distance L^*. Solutions of this type were first computed numerically by Pierrehumbert & Widnall (1981) and Saffman & Szeto (1981). Since these vortices are spatially periodic and do not translate, we must construct the vortex spacing-energy plot $(L^*, \partial E^*/\partial L^*)$, as explained in § A.4. In the case of well-separated vortices (that is, $L^* \gg 1$), it is easy to see that the flow is at an energy maximum, if superharmonic perturbations are considered (see Luzzatto-Fegiz & Williamson 2012). By building the plot shown in figure 9(*a*) for the basic family, we immediately detect the addition of a positive-signature mode at a turning point in L^*.

To introduce an imperfection in this periodic flow, we employ a two-step process, as shown in figure 9(*b–d*). Firstly, we place a point vortex at the saddle-type stagnation point between the vortices (highlighted by a grey box in figure 9*b*). This changes the local flow field, turning each original *saddle* into a *centre*, and creating two new saddle-type stagnation points in its neighbourhood, as exemplified in figure 9(*c*).

Depending on the sign of the point vortex, the new stagnation points are along a line that is either parallel to the vortex row (for $\Gamma_{PV}/\Gamma > 0$, shown in c), or orthogonal to it (for $\Gamma_{PV}/\Gamma < 0$; this is not shown here). Therefore, by introducing an additional point vortex at one of these new stagnation points, we can break either the left/right or top/bottom symmetry in the figure, respectively.

We found that introducing these imperfections does not lead to new bifurcated branches for the linear array. These stability are consistent with the linear analysis of Kamm (1987).

4.5. *The finite-area von Kármán vortex street*

Saffman & Schatzman (1981, 1982) computed steady flows obtained by replacing each point vortex, in a von Kármán street, with a finite-area vortex. In their studies, closely spaced vortices proved prohibitively expensive to resolve, and were not computed.

Following steps similar to those in Luzzatto-Fegiz & Williamson (2011*b*), it can be shown that a street of well-separated vortices is an energy maximum, with a given impulse, if only superharmonic perturbations are considered. In the example considered here, the calculations are performed by choosing a specific value of the impulse $I^* = 0.4$, and computing steady flows as L^* is varied. The basic family of solutions is shown in figure 10(*a*).

The imperfection is constructed by following again the procedure employed for a single row of vortices. It can be shown that, for vortices in a periodic strip that translate along a straight path, the total circulation must be zero (Meiron *et al.* 1984). Therefore, the size of the vortex in the top row was reduced to ensure that the total circulation in the periodic strip remained zero. Following the imperfect solution branch leads to a bifurcation, occurring after the turning point in L^* described above; this is shown in figure 10(*c*). We should note that the turning point in the imperfect branch shown in figure 10(*c*) persists even if a single point vortex is employed to set up the imperfection; in this figure, a single point vortex with strength $\Gamma_{PV}/\Gamma_1 = 10^{-4}$ was used.

Past studies of the stability of the finite-area von Kármán street have focused on the behaviour of subharmonic modes for well-separated vortices (Meiron *et al.* 1984, and references therein). To the best of our knowledge, the stability boundaries that we describe in this section are new. As a check, we also performed a linear stability analysis; eigenvalues are reported in appendix B. We should also remark that the stability properties of the street change, as one examines streets with different impulse I^*; this is discussed in a forthcoming paper (Luzzatto-Fegiz & Williamson 2012).

4.6. *Distributed vortices: the Chaplygin–Lamb dipole*

We examine here the properties of a more realistic representation of a vortex pair, and consider the symmetric, translating pair solution that was described independently by Chaplygin (1903) and Lamb (1932), which involves an analytic representation of a steady, smooth vorticity distribution extending over a finite region (see also Meleshko & van Heijst 1994). In order to construct an IVI diagram for this flow, we must *embed* the Chaplygin–Lamb dipole into a family of solutions that has been constructed through incompressible, isovortical rearrangements. This family of solutions would connect the Chaplygin–Lamb solution with a steady flow given by two well-separated vortices.

We choose to approximate each vortex by a set of nested, uniform-vorticity regions. The discretization is constructed using the procedure described by Legras & Dritschel (1993), who showed that using eight contours for a vortex with compact support yields an excellent approximation for the dynamics of the flow. Once all of the areas A_i and

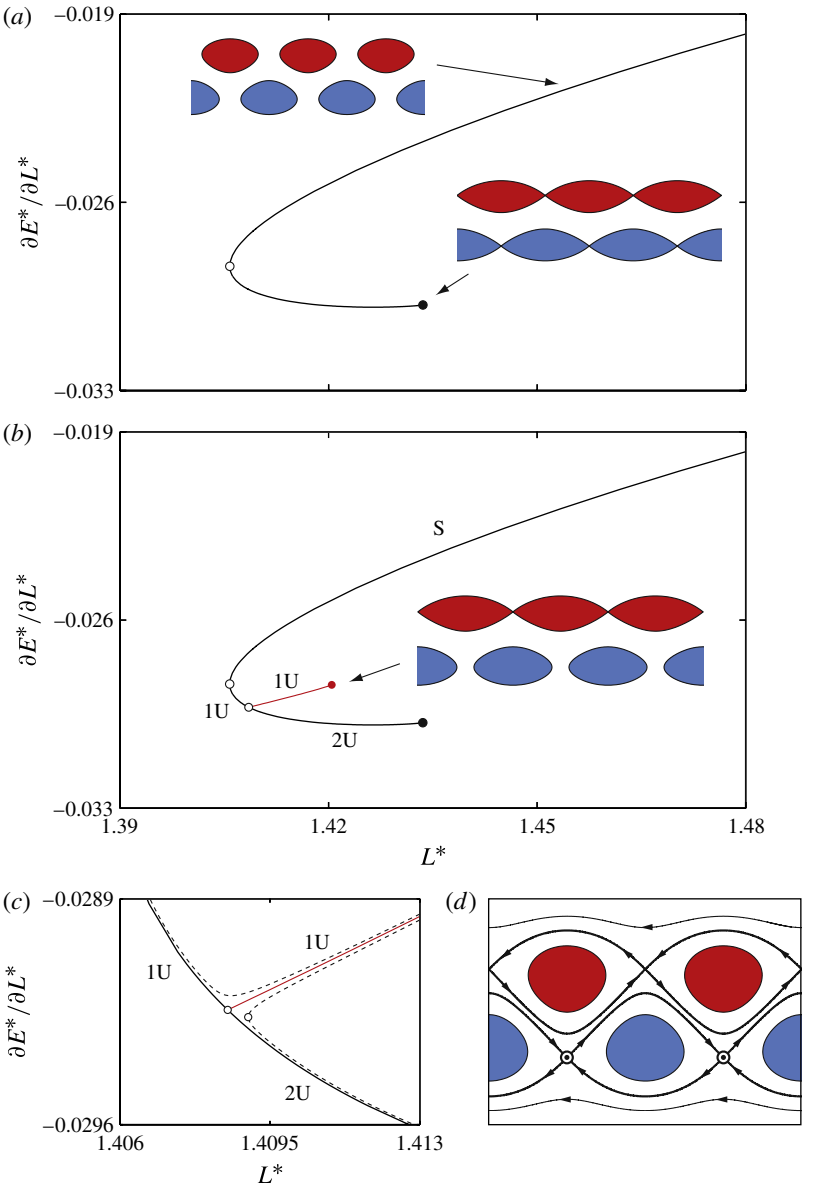

FIGURE 10. Stability diagram for the von Kármán street, for varying L^*, and fixed impulse $I^* = 0.4$. The imperfection is constructed by introducing a weak point vortex at one of the stagnation points marked by a bull's eye in (*d*). Re-computing the steady states, we find that the solution family is broken into two distinct branches (shown by the dashed lines in *c*).

vorticity jumps $\Delta\omega_i$ are computed (with $i = 1, 2, \ldots, 8$), keeping all A_i, $\Delta\omega_i$ constant along the family is sufficient to ensure that the solutions can be traversed through incompressible, isovortical rearrangements.

The basic family of steady flows that we computed is shown in the velocity-impulse diagram in figure 11. For reference, the same figure also displays (with a bull's eye) the impulse and velocity for the exact Chaplygin–Lamb dipole. Note that the

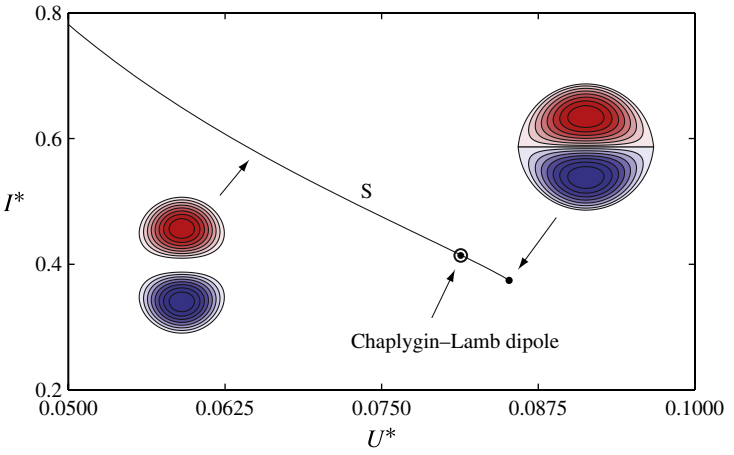

FIGURE 11. Velocity-impulse diagram for the family of distributed vortices based on the Chaplygin–Lamb dipole. The vorticity distribution is approximated using a collection of nested uniform vortices. Introducing an imperfection does not yield any bifurcations, at least up to $U^* \approx 0.083$. The original Chaplygin–Lamb dipole is marked by a bull's eye.

original solution is remarkably close to the approximate family (for the same velocity U^*, the impulse difference is $I^* - I^*_{Lamb} = 7.7 \times 10^{-4}$, or $\sim$0.2 %), which suggests that the integral properties of the configuration are represented very accurately. The imperfection is constructed as in § 4.3, through the combined introduction of a point vortex at one of the saddle-type stagnation points, and the shrinking of the area of one of the outermost vortex patches. While we computed imperfect branches with a variety of point vortex strengths (in the range $\Gamma_{PV}/\Gamma_1 = 10^{-4}$–$10^{-2}$), we did not find any bifurcation, at least up to $U^* \approx 0.083$ (past the Chaplygin–Lamb approximation), after which the numerical procedure for the imperfect system converged very slowly to a steady solution. To interpret these results, it may be helpful to note that, in separate calculations, we found that progressively increasing the number of contours (starting with the uniform pair of § 4.3) shifted the bifurcation of figure 8 progressively closer to the end of the family.

If one were to assume that our calculations can capture all bifurcations, the absence of turning points in I^*, or bifurcations, before the bull's eye in figure 11 would lead to the conclusion that the discretized version of the Chaplygin–Lamb dipole is stable. This suggests that the original, smooth solution should also be stable, at least in a global sense. Of course, one may expect that the lowest vorticity levels (not represented in our discretization) may be rapidly stripped from the configuration through the neighbourhood of the rear stagnation point.

We should note that there is evidence from *viscous* simulations that certain flows with non-zero linear impulse may spontaneously evolve towards a state close to the Chaplygin–Lamb dipole, which would suggest that this solution is at least robust under viscous evolution (e.g. Delbende & Rossi 2009, and references therein). However, to the best of our knowledge, no linear stability analysis has been performed on this flow before (as noted, for example, by Waite & Smolarkiewicz 2008). Surprisingly, the analysis presented here appears to be the first stability result for a discretized Chaplygin–Lamb dipole.

As a check, we also performed a linear stability analysis of this flow; the results are consistent with our IVI diagram, and are reported in appendix B.

5. Stability of steep gravity waves from velocity-impulse diagrams

To highlight the fact that the IVI diagram technique can be applied to other conservative flows for which steady states are associated with a variational principle, we briefly consider here steep gravity waves on the surface of a homogeneous, irrotational fluid of infinite depth. For this flow, a variational principle follows directly from the Hamiltonian formulation of Zakharov (1968). For fixed wavelength λ, waves that steadily translate with velocity c correspond to a stationary point of the Hamiltonian H, defined such that

$$\delta H = \delta[(T + V) - c\,(P - P_0)] = 0, \tag{5.1}$$

where T and V are the kinetic and potential energy, respectively, and P is the wave impulse per unit wavelength, given by $P = \lambda^{-1} \int u \,\mathrm{d}A$ (for a fluid of unit density). Since there is a clear correspondence between $(T + V, c, P)$ above and (E, U, I) from appendix A, turning points in wave impulse P are associated with the introduction of a positive-energy mode.

In order to find the shape $y_{surface} = \eta(x)$ for the steady waves, we solve numerically the classic problem involving the steady Bernoulli equation $1/2\,|\boldsymbol{u}(x, \eta(x))|^2 + g\eta(x) - cu(x, \eta(x)) = \text{const.}$ and the kinematic condition $\overline{\psi} = \psi(x, \eta) - c\eta(x) = 0$ at the interface. As discussed in § 4, the numerical method needs to be able to resolve lower-symmetry flows and fine-scale features in the interface; the discretization procedure used is therefore similar to the one employed for the steady vortices (Luzzatto-Fegiz & Williamson 2011*a*). Given an initial guess for $\eta(x)$, the surface velocities are found by solving the Dirichlet problem for $\overline{\psi}$, given $\overline{\psi} = 0$ on the surface (see Longuet-Higgins & Cokelet 1976). We then iteratively adjust η until the steady Bernoulli equation is satisfied.

As is customary, we normalize P and c by the wavenumber $k = 2\pi/\lambda$ and by the gravitational acceleration g, such that $P^* = Pg^{-1/2}k^{3/2}$, $c^* = cg^{-1/2}k^{1/2}$.

5.1. *Superharmonic instabilities of gravity waves*

The basic family of steady solutions, which originates with an infinitesimal wave, and terminates with waves exhibiting a 120° corner (see e.g. Longuet-Higgins & Fox 1978, and references therein), is shown in figure 12(*a*). We consider stability with respect to superharmonic perturbations, that is, disturbances with the same wavelength as the basic flow. A turning point (associated with the introduction of a positive-signature mode) is visible in figure 12(*a*). An imperfection was constructed by introducing a non-uniform surface tension $T = T_0\,\mathscr{F}(\tau)$, where τ is the arclength measured along the surface, $\mathscr{F}(\tau) = \sin(2\pi\,\tau/\tau_{max})$, and $T_0 = 10^{-5}gk^{-2}$. The steady Bernoulli equation is then $1/2\,|\boldsymbol{u}|^2 + g\eta - cu - T\kappa = \text{const.}$, where κ is the signed curvature. No bifurcated branches were found, in agreement with predictions from linear analysis (see Longuet-Higgins 1986). We must also point out that Longuet-Higgins & Fox (1978) showed, using asymptotic techniques, that as the limiting wave is approached, the family of solution meets a countable infinity of turning points in c and P. By examining equations (5.2) and (6.5) in their paper, it is easy to verify that these give rise to a spiral in a velocity-impulse diagram. According to the work in the present paper, each of these turning points corresponds to the addition of a positive-energy mode.

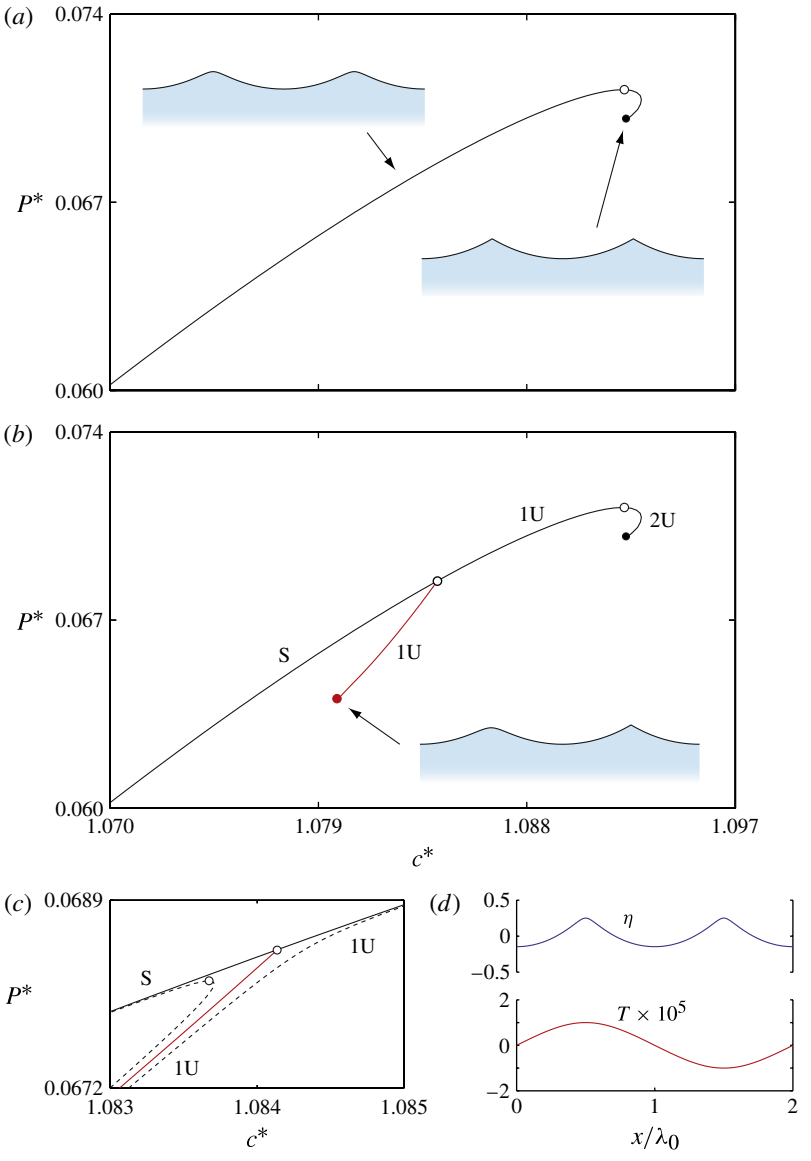

FIGURE 12. IVI diagram for steep gravity waves with phase velocity c^* and impulse P^*. The waves in (*b*) have wavelength $\lambda = 2\lambda_0$, where λ_0 is the wavelength of the original family of solutions shown in (*a*).

We should also note that, for the specific problem of water waves, Longuet-Higgins (1984) showed that turning points in energy coincide with turning points in impulse. The work presented in appendix A of this paper indicates that the link between extrema in impulse and energy also holds for any conservative fluid family constructed from incompressible, isovortical rearrangements.

5.2. *Instabilities for waves with wavelength* $\lambda = 2\lambda_0$

We include two wave crests in our computational domain, and seek solutions with periodicity $\eta(x) = \eta(x + 2\lambda_0)$, which may arise as bifurcations from the original family

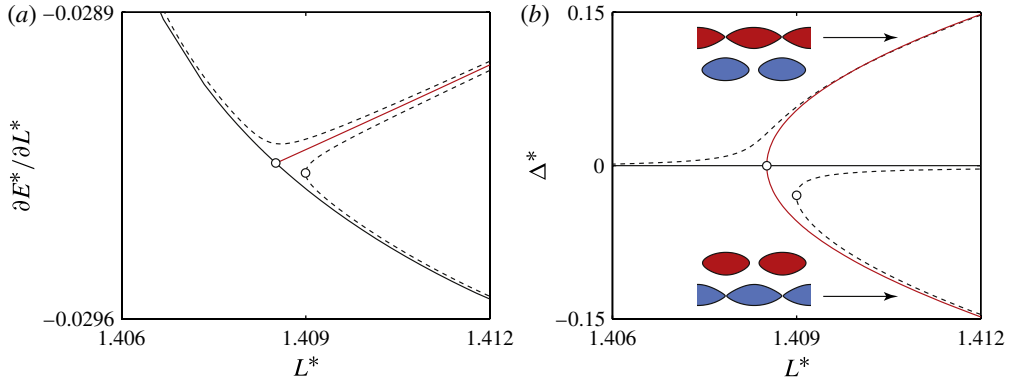

FIGURE 13. Diagram clarifying the nature of some of the bifurcations reported. (*a*) The bifurcation from the family of von Kármán vortices, in an energy-spacing diagram. (*b*) A plot of Δ^*, which is the non-dimensional difference between the perimeter of the top and bottom vortex. The bifurcation can be immediately recognized as a pitchfork.

given by $\eta(x) = \eta(x + \lambda_0)$. Computing the imperfect solutions reveals a turning point in P^* (as shown in figure 12*b,c*). Taking the strength of the surface tension to zero, we recover the bifurcated solution family shown in red in the figure.

The location of this bifurcation, found through the IVI diagram approach, matches the linear stability results of Longuet-Higgins (1978). Subharmonic bifurcations were also previously studied by Chen & Saffman (1980), who computed a substantial portion of this lower-symmetry family of solutions. It appears that the algorithm used by Chen and Saffman was unable to efficiently resolve the lower-symmetry limiting state, which is obtained here for the first time.

6. Discussion

We should comment here on the specific choice of imperfection employed to promote symmetry-breaking. In all of the vortical examples presented here, we make use of weak point vortices, which are introduced at stagnation points of the co-moving flow. We can report that we have also tested several different types of imperfections, including sources and sinks, weak background flows involving simple shear, as well as strain fields of different order (an example of the effect of different background fields on the form of a steady state may be found in Ehrenstein & Le Dizès 2005). While we are not aware of any proof that such imperfections must unfold all bifurcations, we found that all bifurcations were successfully detected in our examples, provided that all of the reflectional and rotational symmetries of the flow were broken. (The absence of undetected bifurcations was checked through linear stability analyses.) The algorithm used to compute the steady states adjusts automatically the step along the solution family between neighbouring steady states (say, Δs), so as to retain a prescribed accuracy in the results; all bifurcations shown were discovered without the need to manually adjust Δs. Once a bifurcation was found, we computed a few additional solutions (with Δs reduced by a factor of $\sim$5) near the turning points, so as to obtain the smooth curves displayed in the insets of figures 6–12.

It may be helpful to show explicitly the correspondence between the patterns arising in an IVI diagram, and those associated with typical bifurcation plots that may be familiar from dynamical systems theory. The IVI diagram in figure 13(*a*) shows

a close-up of the bifurcation encountered for the von Kármán street. By contrast, figure 13(*b*) shows data for the same steady flows in a different plot, where the vertical axis has been replaced by Δ^*, which is the difference between the perimeter of the top and bottom vortex. The point being made here is that, by plotting the same data in a different manner, we can immediately see that this bifurcation is of pitchfork type. The two sides of the fork correspond to vortices that are *mirror* images of one another; these branches are collapsed into a single one in an IVI diagram, as they have the same impulse.

We note that the IVI-diagram technique is comparatively simple to implement, provided one can rely on an efficient numerical procedure to compute the steady states. By comparison, to compute a bifurcated solution branch by approaches traditionally employed in vortex calculations, one needs to first perform a linear stability analysis to find the equilibrium solution for which the exchange of stability occurs. One then must calculate the corresponding eigenmode and superpose it onto the equilibrium solution, using the result as an initial guess for the new branch. It is straightforward to see that, for a wide range of flows, it is significantly easier to instead insert one or more symmetry-breaking flow elements, and compute the imperfect steady states. We should also note here that the use of automated continuation and bifurcation detection packages (such as MatCont or AUTO; e.g. Doedel 1981) does not seem to have been explored so far in vortex flows, and may also prove useful in future work.

Finally, we must be careful to point out that the development of a saddle in the energy surface (as detected by an IVI diagram) is, strictly speaking, only necessary for linear instability; this indicates that an IVI diagram may overestimate the number of linearly unstable modes for an equilibrium. However, for all examples considered in this paper, the number of positive-energy modes from the IVI diagrams matches the number of unstable modes from linear analysis.

7. Concluding remarks

In this paper, we take as a starting point a variational argument that has its roots in the work of Lord Kelvin, and build on ideas from dynamical systems theory and imperfection theory to show that the number of positive energy modes (which are necessary to yield instability) can be detected directly from families of equilibrium solutions.

We address the first issue raised by Dritschel (1985) with respect to the possible use of bifurcation diagram namely, that a link between turning points and stability has not previously been established. In this paper, we develop a turning point approach for vortex flows, which demonstrates a correspondence between folds in impulse and the onset or disappearance of a positive energy mode, thereby bounding the number of linearly unstable modes. In addition, we demonstrate that one can use the shape of a velocity-impulse diagram to infer whether a positive energy mode is lost or gained at the turning point.

Dritschel (1985) also brought attention to the fact that, in the presence of undiscovered bifurcations, a simple turning point approach would fail to capture all exchanges of stability. We address this second issue by introducing symmetry-breaking imperfections in these conservative fluid problems, thereby computing families of imperfect steady states. In all examples considered here, this methodology enables us to detect bifurcations to new families of steady solutions, therefore uncovering the associated changes in stability properties. In all cases, linear analysis confirms that no bifurcations are missed.

A separate issue discussed here concerns the definition of a 'proper' family of fluid solutions. We show that solution families must be built from incompressible, isovortical rearrangements. It is important to note that several existing families of analytical solutions (e.g. Stuart 1967; Mallier & Maslowe 1993) do not satisfy this requirement. Therefore their stability may not be determined by simply seeking turning points in some control parameter for the analytical family (this is different from what has been previously suggested; see Saffman 1992). Instead, in order to determine stability, one must embed an equilibrium flow into a properly constructed family of solutions.

We apply the IVI diagram stability methodology to a wide range of two-dimensional classical flows. Where linear stability results are available, the stability boundaries and number of unstable modes delivered by the IVI diagrams agree precisely with data in the literature. We also consider flows for which a corresponding linear analysis has not yet been performed; for these problems, we obtain what are, to the best of our knowledge, the first available stability results. These new findings include the stability boundaries and bifurcated branches for a finite-area von Kármán street subject to superharmonic perturbations, as well as the result that a discretized Chaplygin–Lamb dipole is stable.

For most of the flows examined, the introduction of imperfections leads us to the discovery of new families of steady solutions, which exhibit lower symmetry. The stability of these new equilibrium flows also follows from the application of the IVI diagram technique. Among the new flows presented here, we discover steady vortices that do not exhibit any reflectional or rotational symmetry, and find *non-symmetric*, equal-area vortex pairs that translate along a straight path. These results also enable us to resolve an outstanding question on the structure of families of opposite-sign vortex pairs, thereby reconciling results for translating and rotating pairs.

The examples considered here are two-dimensional; nevertheless, the turning point approach in § A.2 is formulated for three-dimensional flows. It is generally accepted that three-dimensional inviscid equilibria are saddles of the energy (e.g. Arnol'd 1966), implying that a turning-point approach may be less useful for three-dimensional problems. However, the IVI diagram approach may prove valuable for three-dimensional flows where motion along one or more dimensions is constrained (such as, for example, in certain rotating or stratified flows).

A number of interesting questions remain to be pursued. It would be valuable to obtain a rigorous proof clarifying what types of imperfection can be expected to unfold all bifurcations. Another direction for future work concerns the development of numerical approaches for steady vortices with smooth vorticity distributions. Indeed, even in two dimensions, methods that can compute non-symmetric, smooth vortices from isovortical rearrangements have yet to be formulated (Flierl & Morrison 2011).

In conclusion, we should emphasize that the IVI diagram methodology is obviously not meant to replace other stability approaches, such as linear analysis or simulation, which can be used to yield, for example, growth rates and long-term evolution. Of course, the methodology presented here may be employed in combination with other, possibly more involved, stability approaches.

Acknowledgements

We would like to thank Professor S. Leibovich and Professor P. Steen for interesting and enjoyable discussions. We would like to also thank the anonymous

referees for their helpful comments, which resulted in substantial improvements in the manuscript.

Appendix A. Turning points in vortex flows

A.1. *Kelvin's argument*

For completeness, we recapitulate here the essential steps underlying the mathematical formalization of Kelvin's argument (for a more detailed description, see e.g. Fukumoto & Moffatt 2008). Consider the vorticity functional

$$H = E[\boldsymbol{\omega}] - \boldsymbol{U}\cdot\boldsymbol{I}[\boldsymbol{\omega}] - \boldsymbol{\Omega}\cdot\boldsymbol{J}[\boldsymbol{\omega}], \tag{A 1}$$

where E is the excess kinetic energy, $\boldsymbol{U}$ and $\boldsymbol{\Omega}$ are the linear and angular velocities of the vortex configuration, and $\boldsymbol{I}$ and $\boldsymbol{J}$ are the linear and angular impulses, given by

$$E[\boldsymbol{\omega}] = \frac{1}{2}\int \boldsymbol{\omega}\cdot\boldsymbol{A}\,\mathrm{d}V, \quad \boldsymbol{I}[\boldsymbol{\omega}] = \frac{1}{(D-1)}\int \boldsymbol{r}\times\boldsymbol{\omega}\,\mathrm{d}V, \quad \boldsymbol{J}[\boldsymbol{\omega}] = -\frac{1}{2}\int \boldsymbol{\omega}\,|\boldsymbol{r}|^2\,\mathrm{d}V, \tag{A 2}$$

where $\boldsymbol{r}$ is the position vector, $\boldsymbol{\omega}$ is the vorticity, $\boldsymbol{A}$ is the vector potential (such that $\boldsymbol{u} = \boldsymbol{\nabla}\times\boldsymbol{A}$) and D is the number of dimensions (two or three). If the configuration has zero net circulation, it is possible to choose axes such that $\boldsymbol{J} = \boldsymbol{0}$ (Saffman 1992); similarly, if the net circulation is finite, one can choose the origin such that $\boldsymbol{I} = \boldsymbol{0}$. For brevity, consider here only the first case (similar steps can be followed for configurations with finite circulation). Without loss of generality, choose axes such that $\boldsymbol{J} = (0, 0, J)$, and write $\boldsymbol{\Omega}\cdot\boldsymbol{J} = \Omega J$ in (A 1).

One may seek a stationary point of H for either fixed Ω, or fixed J. Here, we fix J as the control parameter, and require it to take the prescribed value J_0. As is commonly done in variational calculus (e.g. Lanczos 1986), to seek a stationary point of H one must therefore write

$$H = E[\boldsymbol{\omega}] - \Omega(J[\boldsymbol{\omega}] - J_0), \tag{A 3}$$

take the variations in $\boldsymbol{\omega}$ and Ω, and set each independently to zero:

$$\delta\boldsymbol{\omega} : \delta E[\boldsymbol{\omega}] - \Omega\delta J[\boldsymbol{\omega}] = 0 \tag{A 4}$$

$$\delta\Omega : J[\boldsymbol{\omega}] - J_0 = 0. \tag{A 5}$$

Equation (A 5) states that $J[\boldsymbol{\omega}]$ is prescribed, as required. If the $\delta\boldsymbol{\omega}$ variation is assumed isovortical, the components of $\delta\boldsymbol{\omega}$ are not independent, and (A 4) needs to be manipulated further. Let us briefly point out that the isovortical condition is equivalent to writing

$$\delta\boldsymbol{\omega} = \boldsymbol{\nabla}\times(\delta\boldsymbol{\ell}\times\boldsymbol{\omega}), \tag{A 6}$$

where $\delta\boldsymbol{\ell}(\boldsymbol{x})$ is a displacement field through which the variation is enacted (a detailed derivation of (A 6) may be found in Lynden-Bell & Katz 1981). If the flow is incompressible, the components of $\delta\boldsymbol{\ell}$ are also not independent, and one must write

$$\delta\boldsymbol{\ell} = \boldsymbol{\nabla}\times\delta\boldsymbol{a}, \tag{A 7}$$

where the components of $\delta\boldsymbol{a}$ are independent. One can then proceed to show that (A 4), with arbitrary $\delta\boldsymbol{a}$, yields the steady vorticity equation for flow in a frame of reference rotating with angular velocity Ω (see Saffman 1992; Fukumoto & Moffatt 2008 give the corresponding derivation for a translating configuration).

A.2. *Turning points in impulse and the introduction of positive-signature modes*

We now proceed to obtain the stability result linking turning points in impulse with the appearance of positive-signature modes. To assist with the following manipulation, we rewrite the stationarity condition $\delta H = 0$ as

$$\delta H = \int \sum_{i=1}^{4} \frac{\partial \hat{H}}{\partial q_i} \delta q_i \, \mathrm{d}V = 0, \tag{A 8}$$

where $q = (\boldsymbol{\omega}, \Omega)$ and $H \equiv \int \hat{H} \, \mathrm{d}V$. Introduce an auxiliary parameter s, assumed to increase monotonically along a solution branch, such that we may characterize the solution family by $[q_0(s), J_0(s)]$, where the zero subscript denotes an equilibrium value. Differentiate (A 8) along the solution branch:

$$\frac{\mathrm{d}}{\mathrm{d}s}(\delta H) = \int \sum_{i,j=1}^{4} \frac{\partial^2 \hat{H}}{\partial q_i \partial q_j} \delta q_i \dot{q}_j \, \mathrm{d}V + \dot{J}_0 \int \sum_{i=1}^{4} \frac{\partial^2 \hat{H}}{\partial q_i \partial J_0} \delta q_i \, \mathrm{d}V = 0, \tag{A 9}$$

where a dot denotes differentiation with respect to s. We now specialize the above equation to the case $\delta q = \dot{q}$. Since δq is (from Kelvin's argument) an isovortical, incompressible rearrangement, and $\dot{q}$ is a rearrangement along the solution family, this implies that the family of solutions must be constructed from isovortical, incompressible rearrangements. Then

$$\int \sum_{i,j=1}^{4} \frac{\partial^2 \hat{H}}{\partial q_i \partial q_j} \dot{q}_i \dot{q}_j \, \mathrm{d}V = -\dot{J}_0 \int \sum_{i=1}^{4} \frac{\partial^2 \hat{H}}{\partial q_i \partial J_0} \dot{q}_i \, \mathrm{d}V. \tag{A 10}$$

Note that

$$\int \sum_{i,j=1}^{4} \frac{\partial^2 \hat{H}}{\partial q_i \partial q_j} \dot{q}_i \dot{q}_j \, \mathrm{d}V = \delta^2 H_{\textit{along branch}}, \tag{A 11}$$

$$\int \sum_{i=1}^{4} \frac{\partial^2 \hat{H}}{\partial q_i \partial J_0} \dot{q}_i \, \mathrm{d}V = \frac{\mathrm{d}}{\mathrm{d}s}\left(\frac{\partial H}{\partial J_0}\right) = \dot{\Omega}, \tag{A 12}$$

where we have used $\partial^2 H / \partial J_0^2 = 0$. Substituting (A 11) and (A 12) into (A 10) gives

$$\delta^2 H_{\textit{along branch}} = -\dot{J}_0 \, \dot{\Omega}. \tag{A 13}$$

The second variation of H, taken along a branch, is therefore zero at either a turning point in velocity ($\dot{\Omega} = 0$), or at a turning point in impulse ($\dot{J}_0 = 0$). However, note that a necessary condition, for a physically admissible perturbation, is that angular impulse J must be preserved. To satisfy this requirement we need

$$\int \sum_{i=1}^{4} \frac{\partial \hat{J}}{\partial q_i} \dot{q}_i \, \mathrm{d}V = \frac{\mathrm{d}J}{\mathrm{d}s} = \frac{\mathrm{d}J_0}{\mathrm{d}s} = 0, \tag{A 14}$$

since $J = J_0$ along a solution branch. Therefore the case of interest in (A 13) is $\dot{J}_0 = 0$.

To infer the direction of the change of $\delta^2 H$, differentiate (A 13) with respect to s:

$$\frac{\mathrm{d}}{\mathrm{d}s}(\delta^2 H_{\textit{along branch}}) = -\ddot{J}_0 \, \dot{\Omega} - \dot{J}_0 \, \ddot{\Omega}. \tag{A 15}$$

At $\dot{J}_0 = 0$,

$$\frac{\mathrm{d}}{\mathrm{d}s}(\delta^2 H_{along\ branch}) = -\ddot{J}_0\,\dot{\Omega}. \tag{A 16}$$

Equation (A 16) enables us to detect the direction of the change of $\delta^2 H$, from the shape of a velocity-impulse plot, as illustrated schematically in figure 3.

We should note that many turning-point results have appeared previously in other areas of mathematics and mechanics (Poincaré 1885; Katz 1978; Thompson 1979; Maddocks 1987). However, to the best of our knowledge, this is the first work to clarify that, for vortex flows, families of solutions must be constructed from isovortical and incompressible rearrangements, and that the impulse is the correct control parameter.

A.3. *The link between turning points in impulse and turning points in energy*

Past studies of steady uniform vortices have found numerically that turning points of energy coincided with turning points in impulse, to the accuracy of the calculations performed (Saffman & Szeto 1980; Dritschel 1985; Kamm 1987; Dritschel 1995). In fact, there is a simple analysis that can be used to show that $\dot{E} = 0$ and $\dot{J} = 0$ must occur simultaneously, as we explain here.

Consider a family of solutions constructed from incompressible, isovortical rearrangements, and let us write $E = \int \hat{E}\,\mathrm{d}V, J = \int \hat{J}\,\mathrm{d}V$. Then the stationarity condition $\delta H = 0$ can be expressed as

$$\int \sum_{i=1}^{3} \frac{\partial \hat{E}}{\partial \omega_i}\delta\omega_i\,\mathrm{d}V = \Omega \int \sum_{i=1}^{3} \frac{\partial \hat{J}}{\partial \omega_i}\delta\omega_i\,\mathrm{d}V + \delta\Omega(J - J_0). \tag{A 17}$$

Along a solution family, $J - J_0 = 0$, and we can choose $\delta\omega = \dot{\omega}$, such that

$$\dot{E} = \Omega\dot{J}. \tag{A 18}$$

Therefore (provided $\Omega \neq 0$) a turning point in impulse must correspond to an extremum in energy. In an impulse-energy plot, this gives rise to a cusp for any family of solutions constructed through incompressible, isovortical perturbations.

A.4. *Alternative parametrization for spatially periodic flows*

We briefly consider here the special case of flows that are periodic in one space direction (say, x), such that for any flow property ϕ we can write $\phi(x, y, z) = \phi(x + L, y, z)$, where L is the width of the periodic strip. It can be shown that the mathematical formulation of Kelvin's argument discussed in § A.2 also holds for spatially periodic flows, provided the displacement field employed to take the variation is also periodic. Furthermore, simple physical arguments dictate that steady flows in a periodic strip must either translate or be stationary (see Meiron *et al.* 1984). The absence of any rotating equilibria implies that (Ω, J) are irrelevant, and any steady state is associated with

$$\delta H = \delta[E - U(I - I_0)] = 0. \tag{A 19}$$

For these flows, we may apply the velocity-impulse approach introduced earlier in § A.2, by simply considering families of solutions with $L =$ constant. However, for any flow with non-zero overall circulation over one cell of width L (such as, for example, a row of identical vortices), the linear impulse can always be made to vanish by placing the coordinate origin at the vorticity centroid (see e.g. Saffman 1992).

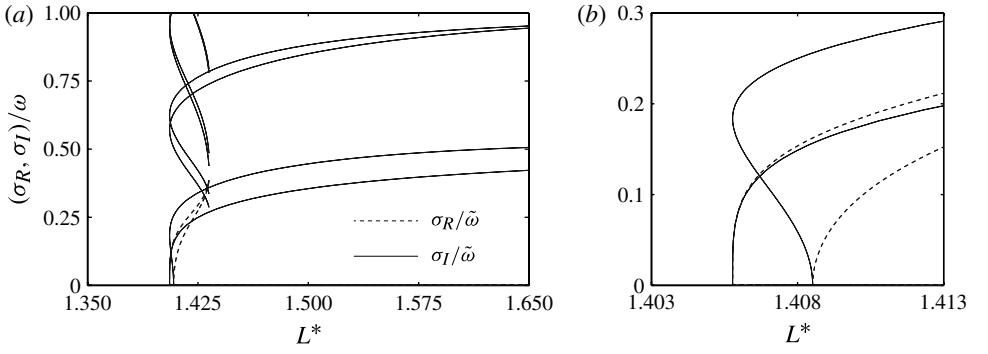

FIGURE 14. Eigenvalues for the basic branch of the finite-area von Kármán street: (*a*) overall view; and (*b*) close-up of the two exchanges of stability.

Therefore, for a wide class of flows, one cannot use turning points in I_0 for stability purposes. Furthermore, even for flows with non-zero impulse (such as a von Kármán vortex street) it may be advantageous to be able to parametrize the solution family by L, instead of I_0. We therefore show here how to recast the turning-point approach in terms of this parameter.

Consider solutions for which I_0 takes a single prescribed value, such that the dependence on the fluid impulse vanishes along the solution family, and such that L may be considered the control parameter. This implies that the flow remains spatially periodic at all times, which in turn requires that any perturbation must have the same periodicity as the original flow (i.e. only superharmonic perturbations are considered). Then, by following steps similar to those in § A.2, with $q = (\boldsymbol{\omega}, U)$, we first find

$$\delta^2 H_{along\ family} = \dot{L} \int \sum_{i=1}^{4} \frac{\partial^2 \hat{H}}{\partial q_i \partial L} \dot{q}_i \, \mathrm{d}V. \tag{A 20}$$

Since the impulse is constant along the family of solutions, we have that $\partial H/\partial L = \partial E/\partial L$. We can therefore write

$$\delta^2 H_{along\ family} = \frac{\mathrm{d}}{\mathrm{d}s}\left(\frac{\partial E}{\partial L}\right)\dot{L}, \tag{A 21}$$

and, differentiating with respect to s,

$$\frac{\mathrm{d}}{\mathrm{d}s}(\delta^2 H_{along\ family}) = \frac{\mathrm{d}}{\mathrm{d}s}\left(\frac{\partial E}{\partial L}\right)\ddot{L} \quad \text{at } \dot{L} = 0, \tag{A 22}$$

which is essentially the same result as in § A.2, with (Ω, J) replaced by $(\partial E/\partial L, -L)$. Therefore, a turning point in L corresponds to the addition or subtraction of a positive-energy mode, as can be inferred from a plot of L and $\partial E/\partial L$.

Appendix B. Stability from linear analysis

For two of the flows that we considered in § 4 (namely, the finite-area von Kármán street and the Chaplygin–Lamb dipole), linear stability results are not available in the literature (for the von Kármán street, Meiron *et al.* 1984 only computed eigenvalues for well-separated vortices). Therefore, as a check on our IVI diagrams, we computed

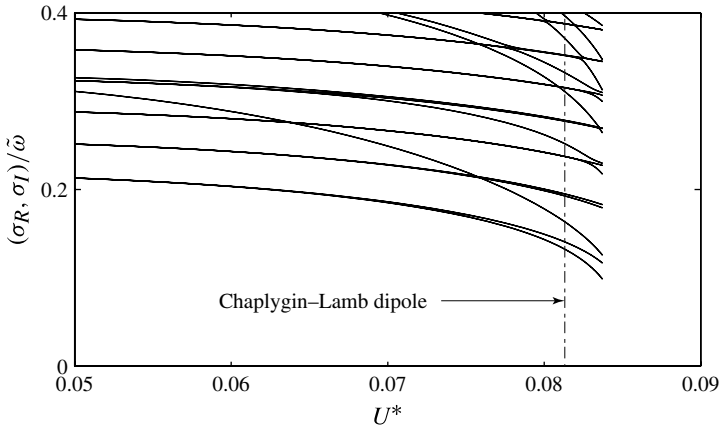

FIGURE 15. Eigenvalues for the family of solutions based on the Chaplygin–Lamb dipole.

eigenvalues associated with perturbations of the form $e^{\sigma t}$ (such that a purely imaginary eigenvalue is spectrally stable). The stability method is reported in Luzzatto-Fegiz & Williamson (2011*a*); its use is also illustrated in Luzzatto-Fegiz & Williamson (2011*b*).

The eigenvalues for the von Kármán street with $I^* = 0.4$ are plotted against L^* in figure 14. Two exchanges of stability are visible, at $L^* = 1.40578$ and 1.40851; these match the stability boundaries from the energy-spacing diagram of figure 10 to six significant figures.

Figure 15 shows eigenvalues for the family of vortices based on the discretized Chaplygin–Lamb dipole. The value of U^* corresponding to the Chaplygin–Lamb solution is marked by a dot-dashed line; all eigenvalues are still purely imaginary at this location, indicating that the discretized flow is spectrally stable, in agreement with the IVI diagram of figure 11.

The von Kármán street calculations used 101 normal modes per vortex, whereas those for the Chaplygin–Lamb dipole used 41 modes for the six innermost vorticity contours, and 101 for the outermost ones. Doubling the number of normal modes for selected cases had no appreciable effect on the eigenvalues reported here. Eigenvalues for solutions near the limiting states require a greater number of normal modes, and are not described here.

REFERENCES

ARNOL'D, V. I. 1965 Conditions for nonlinear stability of stationary plane curvilinear flows of an ideal fluid. *Dokl. Akad. Nauk SSSR* **162**, 773–777.

ARNOL'D, V. I. 1966 Sur un principe variationnel pour les écoulements stationnaires des liquides parfaits et ses applications aux problèmes de stabilité non-linéaires. *J. Méc.* **5**, 29–43.

ARNOL'D, V. I. & AVEZ, A. 1968 *Ergodic Problems of Classical Mechanics*. Benjamin.

BENJAMIN, T. B. 1976 The alliance of practical and analytical insights into the nonlinear problems of fluid mechanics. In *Applications of Methods of Functional Analysis to Problems in Mechanics*, pp. 8–29. Springer.

CASADEMUNT, J. & JASNOW, D. 1991 Defect dynamics in viscous fingering. *Phys. Rev. Lett.* **67**, 3677–3680.

CERRETELLI, C. & WILLIAMSON, C. H. K. 2003 A new family of uniform vortices related to vortex configurations before merging. *J. Fluid Mech.* **493**, 219–229.

CHAPLYGIN, S. A. 1903 One case of vortex motion in fluid. *Trans. Phys. Sect. Imperial Moscow Soc. Friends of Natural Sciences* **11**, 11–14.

CHEN, B. & SAFFMAN, P. G. 1980 Numerical evidence for the existence of new types of gravity waves of permanent form on deep water. *Stud. Appl. Maths* **62**, 1–21.

DEEM, G. S. & ZABUSKY, N. J. 1978 Vortex waves: stationary 'V states', interactions, recurrence, and breaking. *Phys. Rev. Lett.* **40**, 859–862.

DELBENDE, I. & ROSSI, M. 2009 The dynamics of a viscous vortex dipole. *Phys. Fluids* **21**, 073605.

DOEDEL, E. J. 1981 *AUTO: a Program for the Automatic Bifurcation Analysis of Autonomous Systems*. University of Manitoba.

DRITSCHEL, D. G. 1985 The stability and energetics of corotating uniform vortices. *J. Fluid Mech.* **157**, 95–134.

DRITSCHEL, D. G. 1995 A general theory for two-dimensional vortex interactions. *J. Fluid Mech.* **293**, 269–303.

DRITSCHEL, D. G., SCOTT, R. K. & REINAUD, J. N 2005 The stability of quasi-geostrophic ellipsoidal vortices. *J. Fluid Mech.* **536**, 401–421.

EHRENSTEIN, U. & LE DIZÈS, S. 2005 Relationship between corotating vortex-pair equilibria and a single vortex in an external deformation field. *Phys. Fluids* **17**, 074103.

FLIERL, G. R. & MORRISON, P. J. 2011 Hamiltonian-Dirac simulated annealing: application to the calculation of vortex states. *Physica* D **240**, 212–232.

FUKUMOTO, Y. & MOFFATT, H. K. 2008 Kinematic variational principle for motion of vortex rings. *Physica* D **237**, 2210–2217.

HOLM, D. D., MARSDEN, J. E., RATIU, T. & WEINSTEIN, A. 1985 Nonlinear stability of fluid and plasma equilibria. *Phys. Rep.* **123**, 1–116.

JIMÉNEZ, J. 1987 On the linear stability of the inviscid Kármán vortex street. *J. Fluid Mech.* **178**, 177–194.

KAMM, J. R. 1987 Shape and stability of two-dimensional uniform vorticity regions. PhD thesis, California Institute of Technology, Pasadena.

KATZ, J. 1978 On the number of unstable modes of an equilibrium. *Mon. Not. R. Astron. Soc.* **183**, 765–769.

KIRCHHOFF, G. 1876 *Vorlesungen über Mathematische Physik: Mechanik*. Teubner.

LAMB, H. 1932 *Hydrodynamics*. Cambridge University Press.

LANCZOS, C. 1986 *The Variational Principles of Mechanics*. Dover.

LEGRAS, B. & DRITSCHEL, D. G. 1993 Comparison of the contour surgery and pseudo-spectral methods. *J. Comput. Phys.* **104**, 287–302.

LONGUET-HIGGINS, M. S. 1978 The instabilities of gravity waves of finite amplitude in deep water. 2. Subharmonics. *Proc. R. Soc. Lond.* A **360**, 489–505.

LONGUET-HIGGINS, M. S. 1984 New integral relations for gravity waves of finite amplitude. *J. Fluid Mech.* **149**, 205–215.

LONGUET-HIGGINS, M. S. 1986 Bifurcation and instability in gravity waves. *Proc. R. Soc. Lond.* A. **403**, 167–187.

LONGUET-HIGGINS, M. S. & COKELET, E. D. 1976 The deformation of steep surface waves on water. Part 1. A numerical method of computation. *Proc. R. Soc. Lond.* A. **350**, 1–26.

LONGUET-HIGGINS, M. S. & FOX, M. J. H. 1978 Theory of the almost-highest wave. Part 2. Matching and analytic extension. *J. Fluid Mech.* **85**, 769–786.

LOVE, A. E. H. 1893 On the stability of certain vortex motions. *Proc. Lond. Math. Soc.* **25**, 18–42.

LOWRY, B. J. & STEEN, P. H. 1995 Capillary surfaces: stability from families of equilibria with application to the liquid bridge. *Proc. R. Soc. Lond.* A **449**, 411–439.

LUZZATTO-FEGIZ, P. & WILLIAMSON, C. H. K. 2010 Stability of elliptical vortices from imperfect-velocity-impulse diagrams. *Theor. Comput. Fluid Dyn.* **24**, 181–188.

LUZZATTO-FEGIZ, P. & WILLIAMSON, C. H. K. 2011*a* An accurate and efficient method for computing uniform vortices. *J. Comput. Phys.* **230**, 6495–6511.

LUZZATTO-FEGIZ, P. & WILLIAMSON, C. H. K. 2011*b* Resonant instability in two-dimensional vortex arrays. *Proc. R. Soc.* A **467**, 1164–1185.

LUZZATTO-FEGIZ, P. & WILLIAMSON, C. H. K. 2012 Structure and stability of the finite-area Kármán street. *Phys. Fluids* **24**, 066602.

LYNDEN-BELL, D. & KATZ, J. 1981 Isocirculational flows and their Lagrangian and energy principles. *Proc. R. Soc. Lond.* A **378**, 179–205.

MADDOCKS, J. H. 1987 Stability and folds. *Arch. Rat. Mech. Anal.* **99**, 301–328.

MAKAROV, V. G. & KIZNER, Z. 2011 Stability and evolution of uniform-vorticity dipoles. *J. Fluid Mech.* **672**, 307–325.

MALLIER, R. & MASLOWE, S. A. 1993 A row of counter-rotating vortices. *Phys. Fluids* A **5**, 1074–1075.

MEIRON, D. I., SAFFMAN, P. G. & SCHATZMAN, J. C. 1984 The linear two-dimensional stability of inviscid vortex streets of finite-cored vortices. *J. Fluid Mech.* **147**, 187–212.

MELESHKO, V. V. & VAN HEIJST, G. J. F. 1994 On Chaplygin's investigations of two-dimensional vortex structures in an inviscid fluid. *J. Fluid Mech.* **272**, 157–182.

PIERREHUMBERT, R. T. 1980 A family of steady, translating vortex pairs with distributed vorticity. *J. Fluid Mech.* **99**, 129–144.

PIERREHUMBERT, R. T. & WIDNALL, S. E. 1981 The structure of organized vortices in a free shear layer. *J. Fluid Mech.* **102**, 301–313.

POINCARÉ, H. 1885 Sur l'équilibre d'une masse fluide animée d'un mouvement de rotation. *Acta Math.* **7**, 259–380.

POSTON, T. & STEWART, I. 1978 *Catastrophe Theory*. Dover.

SAFFMAN, P. G. 1985 The superharmonic instability of finite-amplitude water waves. *J. Fluid Mech.* **159**, 169–174.

SAFFMAN, P. G. 1992 *Vortex Dynamics*. Cambridge University Press.

SAFFMAN, P. G. & SCHATZMAN, J. C. 1981 Properties of vortex street of finite vortices. *SIAM J. Sci. Stat. Comput.* **2**, 285–295.

SAFFMAN, P. G. & SCHATZMAN, J. C. 1982 Stability of a vortex street of finite vortices. *J. Fluid Mech.* **117**, 171–186.

SAFFMAN, P. G. & SZETO, R. 1980 Equilibrium shapes of a pair of equal uniform vortices. *Phys. Fluids* **23**, 2339–2342.

SAFFMAN, P. G. & SZETO, R. 1981 Structure of a linear array of uniform vortices. *Stud. Appl. Maths* **65**, 223–248.

SAFFMAN, P. G. & TANVEER, S. 1982 The touching pair of equal and opposite uniform vortices. *Phys. Fluids* **25**, 1929–1930.

STOKES, G. G. 1879 Letter to William Thomson. In *The Correspondence between Sir George Gabriel Stokes and Sir William Thomson, Baron Kelvin of Largs* (ed. D. B. Wilson), vol. 2, pp. 470–471. Cambridge University Press (1990).

STUART, J. T. 1967 On finite amplitude oscillations in laminar mixing layers. *J . Fluid Mech.* **29**, 417–440.

THOMSON, W. 1876 Vortex statics. *Proc. R. Soc. Edin.* **9**, 59–73, also *Phil. Mag.* (1880) **10**, 97–109.

THOMSON, W. 1880*a* On maximum and minimum energy in vortex motion. *Nature* **22**, 618–620.

THOMSON, W. 1880*b* Vibrations of a columnar vortex. *Proc. R. Soc. Edin.* **10**, 443–450, also *Phil. Mag.* (1880) **10**, 155–168.

THOMPSON, J. M. T. 1975 Experiments in catastrophe. *Nature* **254**, 392–395.

THOMPSON, J. M. T. 1979 Stability predictions through a succession of folds. *Phil. Trans. R. Soc. Lond.* A **292**, 1–23.

WAITE, M. L. & SMOLARKIEWICZ, P. K. 2008 Instability and breakdown of a vertical vortex pair in a strongly stratified fluid. *J. Fluid Mech.* **606**, 239–273.

ZAKHAROV, V. E. 1968 Stability of periodic waves of finite amplitudes on the surface of a deep fluid. *Zh. Prikl. Mekh. Tekh. Fiz.* **9**, 86–94.